ResearchGate

See discussions, stats, and author profiles for this publication at: https://www.researchgate.net/publication/15329404

An HMG-box-containing T-cell factor required for thymocyte differentiation

Article *in* Nature · April 1995

DOI: 10.1038/374070a0 · Source: PubMed

CITATIONS
487

READS
144

10 authors, including:

Sjef Verbeek
Leiden University Medical Centre
278 PUBLICATIONS **16,341** CITATIONS

SEE PROFILE

Hein Te Riele
Netherlands Cancer Institute
196 PUBLICATIONS **11,506** CITATIONS

SEE PROFILE

Els Robanus-Maandag
Leiden University Medical Centre
50 PUBLICATIONS **9,596** CITATIONS

SEE PROFILE

Marc Van de Wetering
The Princess Máxima Center for Pediatric Oncology
144 PUBLICATIONS **40,639** CITATIONS

SEE PROFILE

Some of the authors of this publication are also working on these related projects:

Project anti-FcgRIIB View project

Project Imaging of Inflammation View project

All content following this page was uploaded by Sjef Verbeek on 21 May 2014.

The user has requested enhancement of the downloaded file.

An HMG-box-containing T-cell factor required for thymocyte differentiation

Sjef Verbeek*, David Izon†, Frans Hofhuis*, Els Robanus-Maandag‡, Hein te Riele‡, Marc van de Wetering*, Mariette Oosterwegel*†, Anne Wilson§, H. Robson MacDonald§ & Hans Clevers*||

* Department of Immunology, University Hospital, PO Box 85500, 3508 GA, Utrecht, The Netherlands
† Division of Immunology, The Netherlands Cancer Institute, Plesmanlaan 121, 1066 CX Amsterdam, The Netherlands
‡ Division of Molecular Genetics, The Netherlands Cancer Institute, Plesmanlaan 121, 1066 CX Amsterdam, The Netherlands
§ Ludwig Institute for Cancer Research, Lausanne Branch, University of Lausanne, 1066 Epalinges, Switzerland
|| To whom correspondence should be addressed

Two candidate genes for controlling thymocyte differentiation, *T-cell factor-1* (*Tcf-1*) and lymphoid enhancer-binding factor (*Lef-1*), encode closely related DNA-binding HMG-box proteins[1,2]. Their expression pattern is complex and largely overlapping during embryogenesis, yet restricted to lymphocytes postnatally[3]. Here we generate two independent germline mutations in *Tcf-1* and find that thymocyte development in (otherwise normal) mutant mice is blocked at the transition from the CD8$^+$, immature single-positive to the CD4$^+$/CD8$^+$ double-positive stage. In contrast to wild-type mice, most of the immature single-positive cells in the mutants are not in the cell cycle and the number of immunocompetent T cells in peripheral lymphoid organs is reduced. We conclude that Tcf-1 controls an essential step in thymocyte differentiation.

Postnatal *Tcf-1* expression in mice is restricted to T lymphocytes[3]. The onset and kinetics of *Tcf-1* expression within the T-cell lineage was determined by northern blot analysis of thymocyte subpopulations which were separated by fluorescence-activated cell sorting (FACS). Thymocytes were sorted on the basis of the differential surface expression of CD25, CD4, CD44, CD8 and CD3, which define an ordered progression along the T-lineage differentiation pathway[4,5]. *Tcf-1* expression peaks in CD8$^+$/CD3$^-$/CD4$^-$ T-cell precursors (immature single-positive cells, ISPs) and declines thereafter (Fig. 1*a*). *Lef-1* messenger RNA is already detectable at the CD25$^+$/CD44$^-$ double-negative (DN) stage and is still present at the double-positive (DP) stage (Fig. 1*b*).

To determine whether TCF-1 plays a role in T-cell development after lineage commitment, two independent mutations were introduced into the *Tcf-1* gene by homologous recombination in embryonic stem (ES) cells (Fig. 2). The Tcf$^{\Delta VII}$ mutation was created by introducing a short deletion into exon VII, which encodes an essential part of the sequence-specific HMG box[6]. The Tcf$^{\Delta V}$ mutation consisted of a small deletion in exon V, which is conserved between *Tcf/Lef* homologues in *Drosophila* (D. Dooijes and H.C., unpublished), mice and man[1,7]. In both cases, homologous recombination occurred with high frequency in ES cells (19 and 37% of G418-resistant clones, respectively).

Mice homozygous for either of the two mutations were healthy and fertile and had a normal lifespan. Apart from the lymphoid system, internal organs showed no gross morphological abnormalities. Heterozygous mice had the wild-type phenotype, including a normal T-lymphocyte differentiation pathway (see Fig. 3*d* for example), arguing against a dominant-negative effect of the mutations.

As shown in Fig. 3*a*, the thymus of Tcf$^{\Delta VII/\Delta VII}$ mice were greatly reduced in size. Histological analysis revealed an organization into cortex and medulla, but the cortex was narrow and pale-staining, indicative of hypocellularity (Fig. 3*b* and *c*). Correspondingly, total thymocyte numbers were reduced 10–100 fold compared to heterozygous or wild-type littermates (Fig. 3*d*), a difference that became more dramatic with age. Tcf$^{\Delta V/\Delta V}$ thymuses were less-affected, with thymocyte numbers decreased by 2–5-fold (Fig. 3*d*) at all ages, and no histological aberrations apart from a moderate reduction in size (not shown).

The reduction in thymocyte numbers in both types of mutant mice suggests that disruption of the *Tcf-1* gene interferes with thymocyte development. To define the stage(s) at which this interference occurs, we analysed thymocytes by triple staining for CD3 (or T-cell receptor α/β chains (TCRα/β)), CD4 and CD8 by FACS. In Tcf$^{\Delta VII/\Delta VII}$ thymuses, we found a largely unaffected CD4/CD8 double-negative precursor population. By contrast absolute numbers of DP and mature single-positive (MSP) thymocytes were reduced up to 100-fold compared to littermate controls (Fig. 4*a*). We consistently observed an

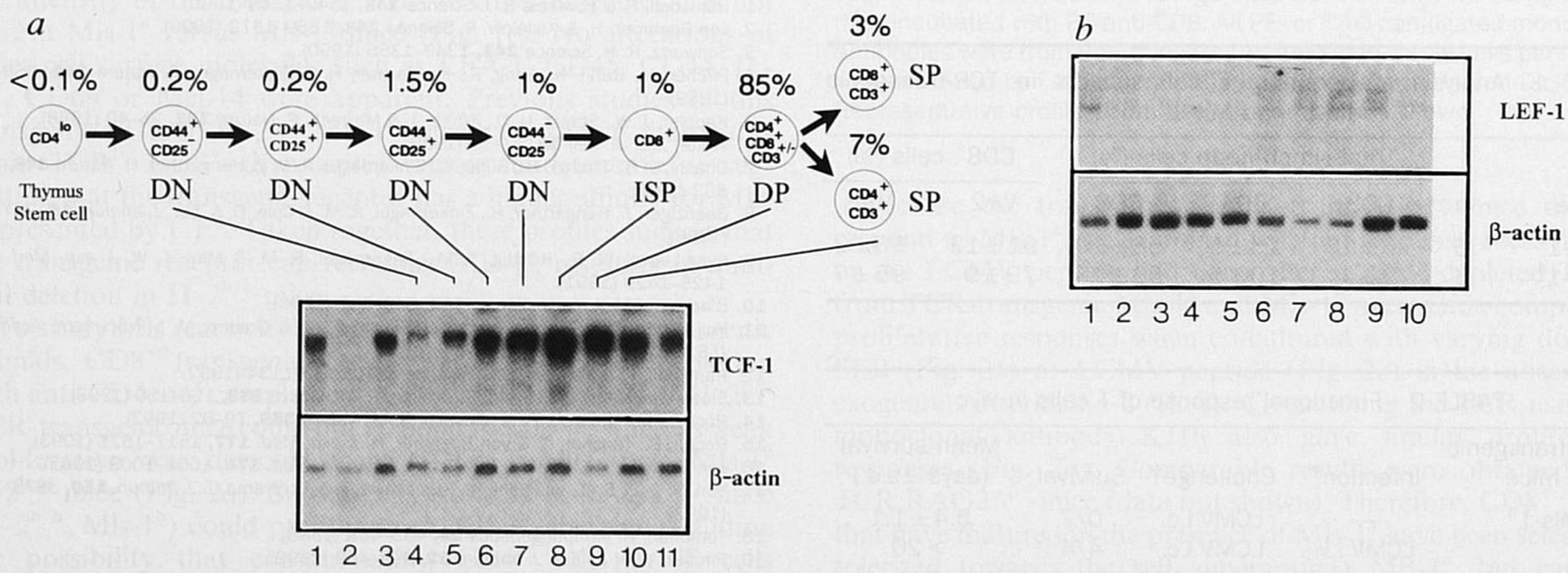

FIG. 1 Stage-specific expression of *Tcf-1* and *Lef-1* mRNA in the T-cell lineage. Surface markers CD44, CD25, CD4, CD8 and TCR/CD3 define an ordered progression in thymocyte differentiation[3] (top). Thymocytes were separated on the basis of the expression of these surface markers, as described[4]. Northern blots were probed for *Tcf-1* and for β-actin as a control. *Tcf-1* expression was highest in ISP and DP RNA samples when normalized for β-actin. *Lef-1* expression, typically appearing as a doublet[2], was much lower and was detectable from the CD25$^+$/CD44$^-$ to the DP stage. Lanes: 1, TCRα/β cytotoxic T-cell clone; 2, P815 non-lymphoid cell line; 3, TCRγ/δ hybridoma; 4–10, sorted thymocytes of phenotypes indicated above the blot; 11, lymph node T cells.

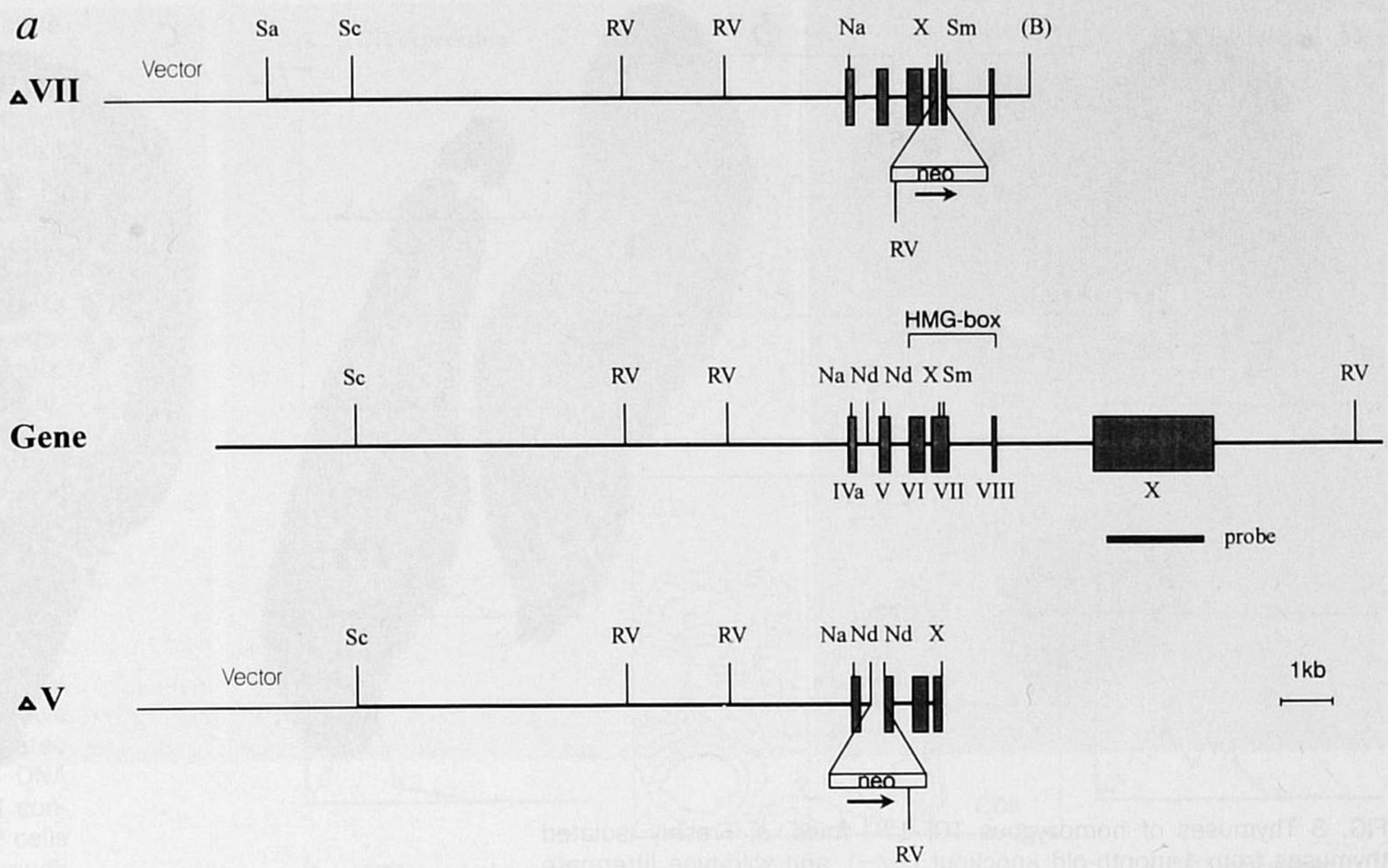

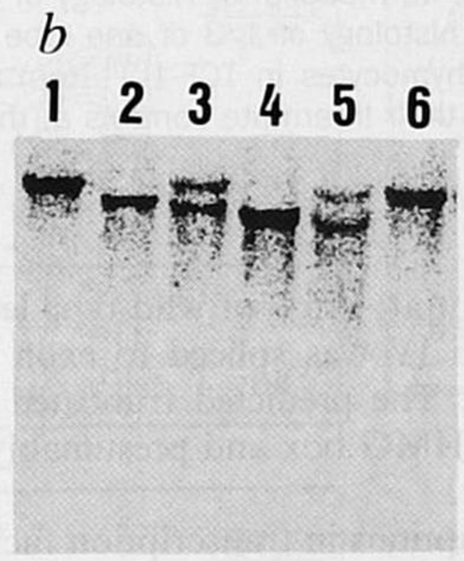

FIG. 2 Disruption of the murine *Tcf-1* gene and genotypic analysis. *a*, Restriction enzyme maps of *Tcf-1* genomic fragment and the two targeting constructs. Exons are indicated as hatched boxes and numbered according to the human *Tcf-1* gene[6]. Exon IVa and IX represent alternative exons. Restriction sites: RV, *Eco*RV; Sc, *Sac*II; X, *Xho*I; Nd, *Nde*I; Na, *Nar*I; Sm, *Sma*I; Ns, *Nsi*I; B, *Bgl*II. *b*, Southern blot analysis of *Eco*RV-digested genomic DNA from adult progeny of intercrosses of either TCF-$1^{\Delta VII}$ or TCF-$1^{\Delta V}$ heterozygotes. A cDNA fragment covering most of exon X was used as a probe. Hybridizing bands of 13, 9 or 10 kb indicate the presence of a *Tcf-1* wild type, Tcf-$1^{\Delta V}$ or Tcf-$1^{\Delta VII}$ alleles, respectively. Lanes: 1 and 6, Tcf-$1^{+/+}$; 2, Tcf-$1^{\Delta VII/\Delta VII}$; 3, Tcf-$1^{\Delta VII/+}$; 4, Tcf-$1^{\Delta V/\Delta V}$; 5, Tcf-$1^{\Delta V/+}$. Correct 5′ integration was confirmed by hybridization with a full-length *Tcf-1* cDNA probe (not shown).

METHODS. Murine *Tcf-1* genomic clones were isolated from a C57/B6 × C3H EMBL3 library (Stratagene) and sequenced by standard procedures. Oligonucleotides were from Isogen, Amsterdam. In a 12-kb *Sal*I–*Bgl*II fragment, a 67-bp *Xho*I–*Sma*I fragment containing part of exon VII was replaced by a PGK-*neo*^{r} cassette. The resulting replacement-type targeting vector pTCF-$1^{\Delta VII}$ was linearized by *Not*I digestion. In a 9-kb *Sac*II–*Xho*I fragment, a 350-bp *Nde*I fragment containing part of intron IV and exon V was replaced by a PGK-*neo*^{r} cassette. The resulting replacement type targeting vector pTCF-$1^{\Delta V}$ was linearized by *Xho*I digestion. For the generation of Tcf-$1^{\Delta VII}$ mutant mice, 2×10^8 E14 ES cells (grown in gelatin-coated Petri dishes in Buffalo rat-liver cell-conditioned medium supplemented with LIF), were electroporated in 600 μl medium (800 V, 3 μF, 0.1 ms) with 150 μg of the TCF-$1^{\Delta VII}$ construct. Targeted cells were selected after one day in 150 μg ml^{-1} G418. From 127 *neo*^{r} clones, 24 (19%) had acquired the *neo*^{r} insertion by homologous recombination. TCF-$1^{\Delta V}$ mutant ES cells mice were obtained in a similar fashion. From 310 *neo*^{r} clones isolated, 106 (37%) had acquired the *neo*^{r} insertion by homologous recombination. Chimaeric animals were generated by injection of heterozygous ES cells into C57B1/6 blastocysts. Germline chimaeras (F_0) were obtained from 2 out of 3 injected TCF-$1^{\Delta V}$ clones and from 3 out of 5 injected TCF-$1^{\Delta VII}$ clones.

increase in the percentage of ISP ($CD8^+/CD3^-/CD4^-$) thymocytes. Absolute numbers of these precursor cells, which normally represent 0.5–1% of total thymocytes[8], were increased 3–5-fold in young (3–6-week-old) mutant mice (not shown). In older mice, total numbers of thymocytes were so low that this effect was less clear. Consistent with the expansion of the DN compartment, the proportion of cells staining for the early markers CD25, CD44 and FcγRII/III was markedly increased (not shown). Phenotypic changes in $Tcf^{\Delta V/\Delta V}$ thymocytes were qualitatively similar but less striking. The size of the DN population was normal, whereas the DP and MSP populations were decreased 3–5-fold, compared to littermate controls, thus accounting for the observed decrease in total thymocytes. The ISP compartment was expanded 3–5-fold in absolute numbers at all ages (Fig. 4*b*).

As expected[8], ISP cells could be stained with the early marker heat-stable antigen (HSA), although not as much as wild-type ISP cells (Fig. 4*c*), probably because of their smaller size, as seen in the scatter profiles (not shown). Staining for intracellular TCR-β protein, indicating productive TCR-β rearrangement, was the same in mutant and wild-type ISP cells (not shown). Determination of DNA content revealed that the vigorous cell-cycling of the normal ISP compartment[8] did not occur in knock-out ISP cells (Fig. 4*c*), thereby accounting for the decrease in cell numbers after the ISP stage in mutant mice.

In $Tcf^{\Delta VII/\Delta VII}$ mice, T-cell numbers in lymph nodes and spleen were decreased 10-fold and 3-fold, respectively; the CD4:CD8 and TCRα/β:TCRγ/δ ratios were unaffected. B-cell numbers were normal, as assessed by staining for soluble immunoglobulin and B220, as were natural killer cells, which were detected with the monoclonal antibody NK1.1 (not shown). In $Tcf^{\Delta V/\Delta V}$ mice, there was no significant decrease in T- or B-cell numbers in spleens or lymph nodes (not shown). Splenic T cells from both $Tcf^{\Delta V/\Delta V}$ and $Tcf^{\Delta VII/\Delta VII}$ mice were functional in proliferation assays in response to concanavalin A and alloantigen, as well as in allogeneic cytotoxicity assays (not shown). Furthermore, total IgM and IgG remained the same, as did specific immunoglobulin responses to foreign protein antigens (M. Schilham, unpublished). Thus, despite the pronounced effect of the $Tcf^{\Delta VII}$ mutation in particular on thymocyte development, mature T lymphocytes did not seem to depend on a functional *Tcf-1* gene product.

The quantitative difference in T-cell numbers correlated with the difference in the amount of mRNA for the two mutant phenotypes. No transcript was detected on a northern blot from the $Tcf^{\Delta VII}$ allele, but a single, novel mRNA from the $Tcf^{\Delta V}$

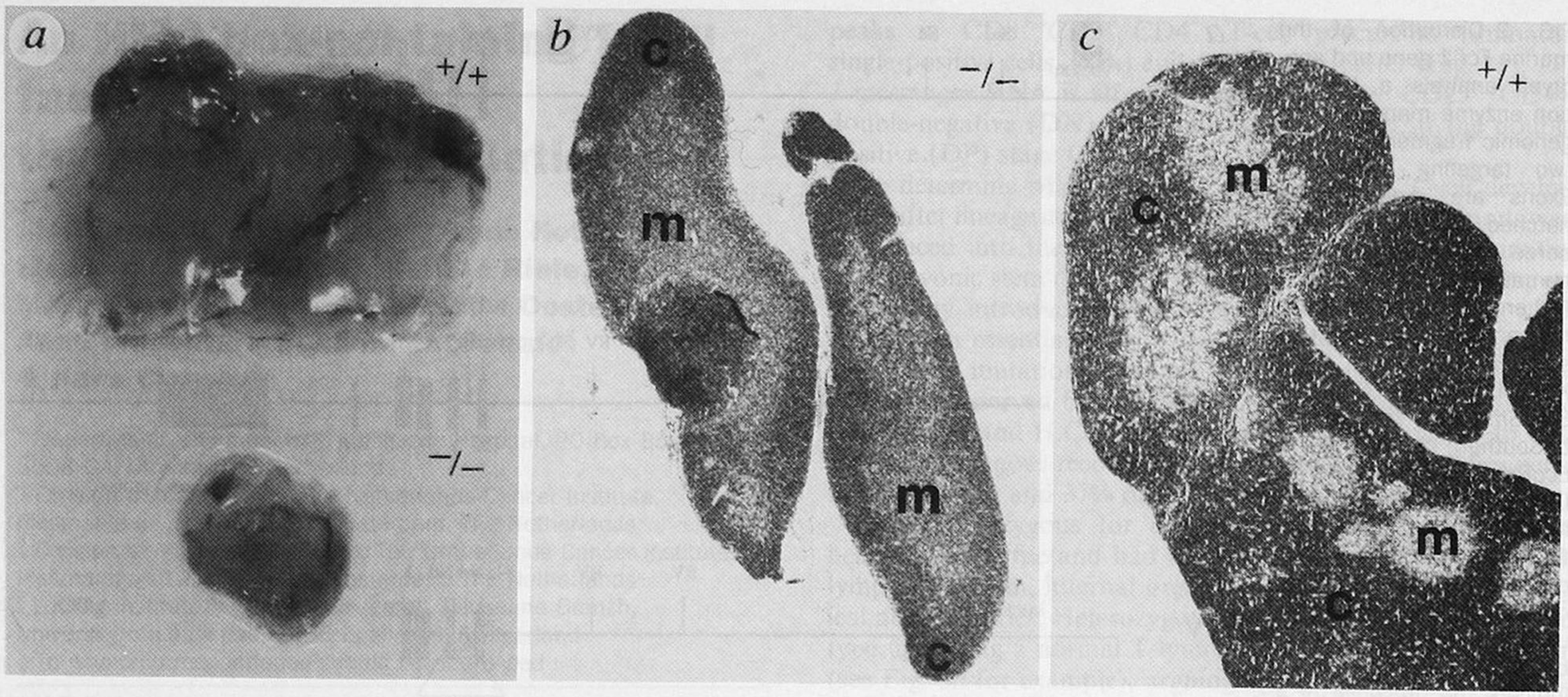

FIG. 3 Thymuses of homozygous TCF-1$^{\Delta VII}$ mice. *a*, Freshly isolated thymuses from 1-month-old knockout (−/−), and wild-type littermate (+/+). *b* and *c*, Histological analysis of thymuses from *a* at equal magnification. C, Cortex; M, medulla. *b*, Histology of two lobes of the TCF-1$^{\Delta VII/\Delta VII}$ thymus; *c*, histology of 1/3 of one lobe of a +/+ thymus. *d*, Total numbers of thymocytes in TCF-1$^{\Delta VII}$ (top) and TCF-1$^{\Delta V}$ (bottom) knockout mice and their littermate controls at the indicated ages.

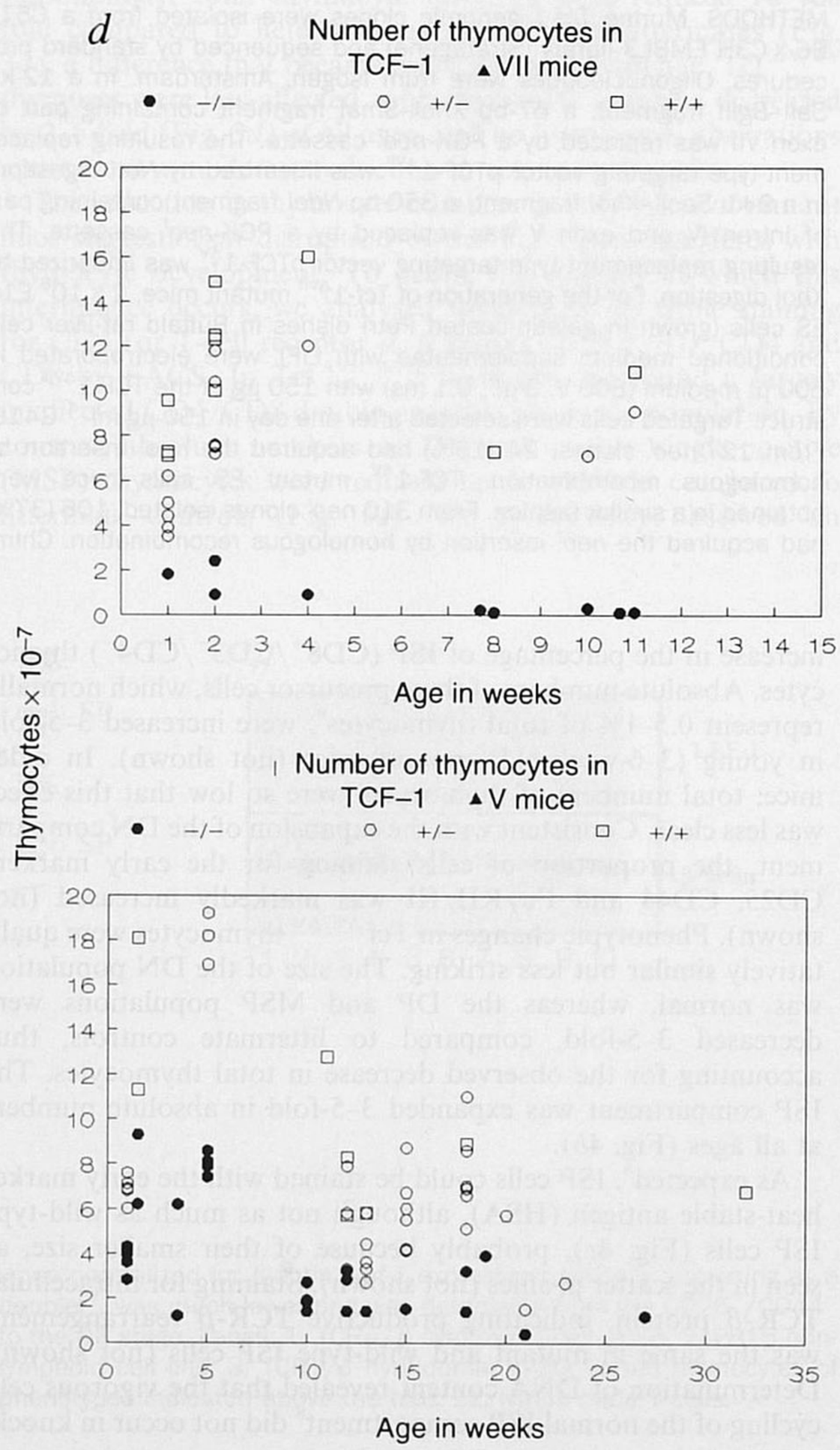

allele was apparent at ~15% of wild-type level (not shown). In this mRNA, exon IV was spliced to exon VI, resulting in an in-frame deletion. The predicted truncated protein retains the sequence-specific HMG box and presumably at least part of its biological activity.

So far, no disruptions in transcription factor genes have been reported that uniquely affect the T-cell lineage. The T lymphocyte has been the focus of many knockout experiments: genes encoding TCR α- and β-chains[9,10], Lck tyrosine kinase[11], Rag recombinases that mediate rearrangement of TCR and immunoglobulin genes[12,13], and accessory surface molecules such as CD4 and CD8α[14,15], have all been disrupted. The resulting phenotypes can be divided into (1) 'early' phenotypes, in which the total number of thymocytes is severely decreased as a result of a block at the DN stage, and (2) 'late' phenotypes, in which numbers of thymocytes are normal because the block is at the DP stage or later. *Tcr-β*, *Rag* and *Lck* gene disruption results in typical early phenotypes[9,11–13]; *Tcr-α*, CD4 and CD8α disruption cause a typical late phenotype[9,10,14,15]. The *Tcf-1* knockout phenotype should be classified as an early phenotype, but is unique in that the block occurs at the ISP-to-DP transition and not in the DN stage. Therefore *Tcf-1* cannot be positioned upstream of the other 'early' genes *Lck*, *Tcr-β* or *Rag-1* and *-2*. Similarly, no simple hierarchical relationship can exist between *Tcf-1* and *Tcr-α* or other late genes, as *Tcf-1* gene disruption would then give a late phenotype.

The molecular events controlled by *Tcf-1* are unknown. Tcf-1 does not behave as a typical transcriptional activator, as measured in cotransfection CAT assays[16]. It contains a DNA-binding HMG box with specificity for the A/T A/TCAAAG-motif, which is present in many T-cell enhancers[17,18]. Sequence-specific HMG-box factors may act as architectural elements to organize the spatial structure of enhancers[20]. *Lef-1* shows identical sequence preference[2] and, given its expression in early thymocytes (Fig. 1*b*), might be responsible for the 'leakiness' of the *Tcf-1* mutation. *Lef-1* gene disruption does not affect the T lineage, but

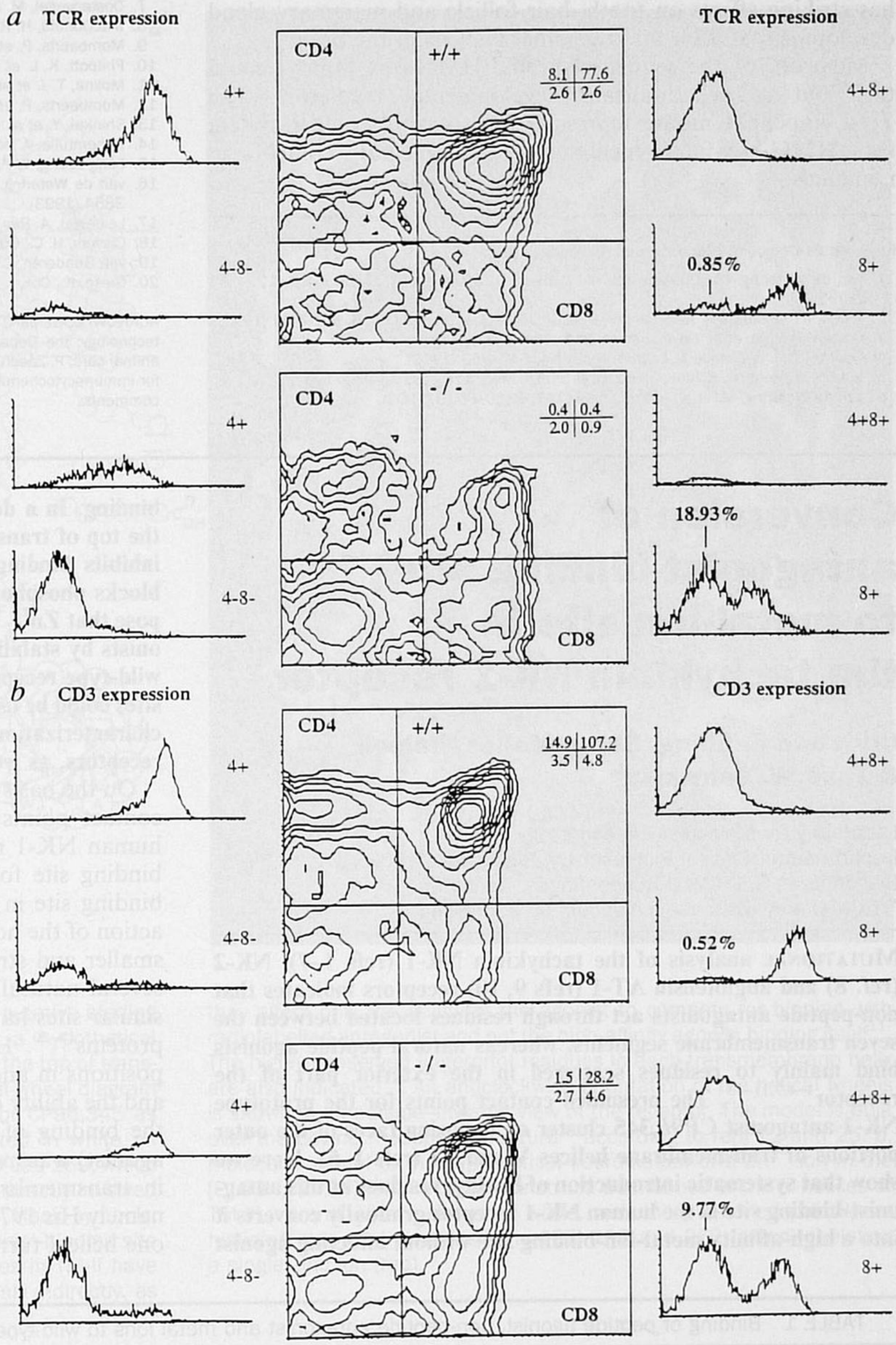

FIG. 4 Phenotypic and cell-cycle analysis of *Tcf-1* knockout thymocytes. *a*, Triple TCR/CD4/CD8 staining of TCF-1$^{\Delta VII}$ thymocytes (bottom) compared to a littermate control (top). Absolute numbers of cells in CD4/CD8 quadrants are given at the top right of each panel. Gates set to analyse TCR expression coincided with the cross set for statistical analysis. TCR or CD3 expression in arbitrary units is given directly adjacent to the pertinent CD4/CD8 quadrant. Percentage of ISP cells are indicated (0.85 and 18.93%, respectively). *b*, As *a*, but for TCF-1$^{\Delta V/\Delta V}$ thymocytes (bottom). *c*, HSA/CD3 surface expression (top) and cell-cycle analysis (bottom) of CD8 single-positive cells in TCF-1$^{\Delta V/\Delta V}$ (left) and wild-type thymocytes (right). HSA^{high}/CD3^{-} are typical ISP cells[8]. HSA^{low}/CD3^{+} cells represent mature single-positive thymocytes. ISP cells in the indicated gates were sorted and their DNA content determined. 32.0% of control versus 5.6% of mutant ISP cells were in S or G2/M phase. Although mature CD8^{+} cells (SP; sorting gate not indicated) were mostly non-cycling, differences were again observed between control and mutant mice.

METHODS. Four-colour staining and FACS sorting was done using the antibody conjugates anti-CD8 Red^{613} (Gibco BRL), anti-CD4 allopycocyanin (Caltag), anti-CD3 FITC (purified and conjugated by A.W. from clone 17A2, and anti-CD24 (HSA) phycoerythrin (Pharmingen). Live gating and sorting on a FACStar^{+} (Becton Dickinson) was done at three levels: for viable cells on FSC and SSC, for CD4^{-}CD8^{+} cells based on FL3 and FL4 and then for the indicated populations of CD24^{+}CD3$^{-/lo}$ (that is, ISP) and CD24$^{-/lo}$CD3^{+} (that is, SP) based on FL1 and FL2. Sorted cells were analysed for DNA content after addition of 250 μg ml^{-1} propidium iodide in 1% NP-40. Percentage S and G2/M cells was determined using the Doublet Discrimination Module on the FACScan. All data were analysed using the Lysys program (Becton Dickinson).

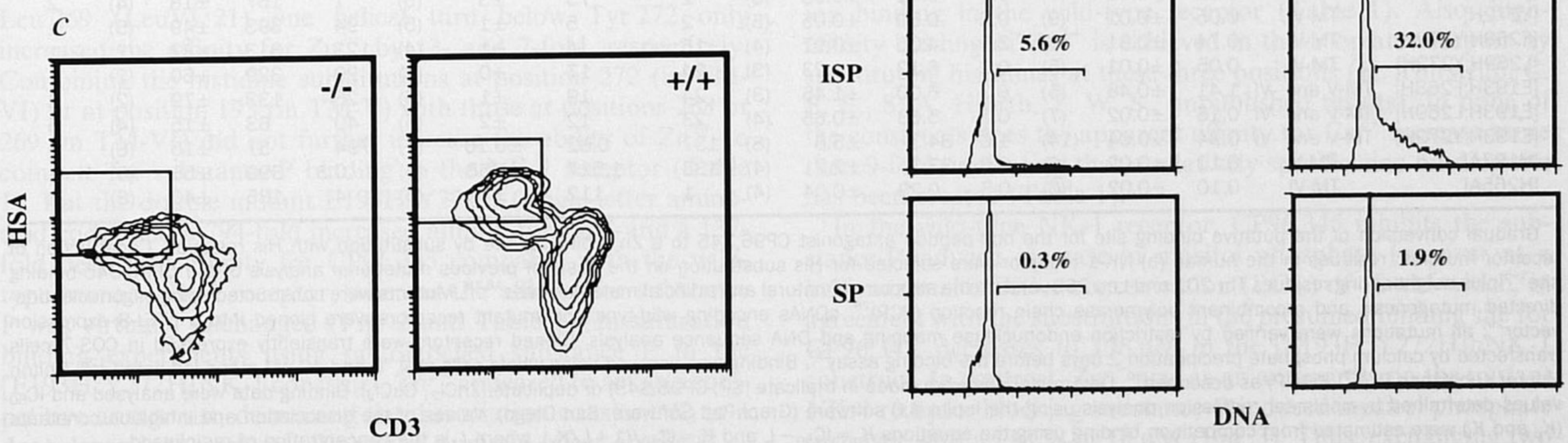

has striking effects on tooth, hair follicle and mammary gland development and on the trigeminal nucleus in the brain[19].

Members of the sequence-specific HMG-box family, could turn out to be important developmental regulators. The *Tcf-1* knockout mouse represents an accessible model system for HMG-box-factor-mediated developmental control in mammals. □

Received 21 October 1994; accepted 10 January 1995.

1. van de Wetering, M., Oosterwegel, M., Dooijes, D. & Clevers, H. *EMBO J.* **10,** 123–132 (1991).
2. Travis, A., Amsterdam, A., Belanger, C. & Grosschedl, R. *Genes Dev.* **5,** 880–984 (1991).
3. Oosterwegel, M. *et al. Development,* **118,** 439–448 (1993).
4. Godfrey, D. I. & Zlotnik, A. *Immun. Today* **14,** 547–553 (1993).
5. Wilson, A., Held, W. & MacDonald, H. R. *J. exp. Med.* **179,** 1355–1360 (1994).
6. van de Wetering, M. *et al. J. biol. Chem.* **267,** 8530–8536 (1992).
7. Oosterwegel, M. *et al. J. exp. Med.* **173,** 1133–1142 (1992).
8. MacDonald, H. R., Budd, R. C. & Howe, R. C. *Eur. J. Immun.* **18,** 519–523 (1988).
9. Mombaerts, P. *et al. Nature* **360,** 225–231 (1992).
10. Philpott, K. L. *et al. Science* **256,** 1448–1452 (1992).
11. Molina, T. J. *et al. Nature* **357,** 161–164 (1992).
12. Mombaerts, P. *et al. Cell* **68,** 869–877 (1992).
13. Shinkai, Y. *et al. Cell* **68,** 855–867 (1992).
14. Rahemtulla, A. *et al. Nature* **353,** 180–184 (1991).
15. Fung-Leung, W-P. *et al. Cell* **65,** 443–449 (1991).
16. van de Wetering, M., Oosterwegel, M., van Norren, K. & Clevers, H. *EMBO J.* **12,** 3847–3854 (1993).
17. Leiden, J. *A. Rev. Immun.* **11,** 539–570 (1993).
18. Clevers, H. C., Oosterwegel, M. A. & Georgopoulos, K. *Immun. Today* **14,** 591–596 (1993).
19. van Genderen, C. *et al. Genes Dev.* **8,** 2691–2703 (1994).
20. Giese, K., Cox, J. & Grosschedl, R. *Cell* **69,** 185–195 (1992).

ACKNOWLEDGEMENTS. We thank A. Berns and members of his laboratory for the ES cell technology; the Department of Pathology for tissue sections; T. Hesp and L. van Essen for animal care; P. Zaech and C. Knabenhans for FACS sorting and cell-cycle analysis; M. Schreyer for immunocytochemistry; and A. Kruisbeek, M. Owen, M. Schilham and R. Grosschedl for their comments.

Conversion of antagonist-binding site to metal-ion site in the tachykinin NK-1 receptor

Christian E. Elling, Søren Møller Nielsen & Thue W. Schwartz*

Laboratory for Molecular Endocrinology,
Department of Clinical Biochemistry, Rigshospitalet 6321,
Blegdamsvej 3, DK-2100 Copenhagen, Denmark
* To whom correspondence should be addressed

MUTATIONAL analysis of the tachykinin NK-1 (refs 1–7), NK-2 (ref. 8) and angiotensin AT-1 (refs 9, 10) receptors indicates that non-peptide antagonists act through residues located between the seven transmembrane segments, whereas natural peptide agonists bind mainly to residues scattered in the exterior part of the receptor[1–4,7,11–13]. The presumed contact points for the prototype NK-1 antagonist CP96,345 cluster on opposing faces of the outer portions of transmembrane helices V and VI (refs 1–5). Here we show that systematic introduction of histidyl residues at this antagonist-binding site in the human NK-1 receptor gradually converts it into a high-affinity metal-ion-binding site without affecting agonist binding. In a double mutant with histidine residues substituted at the top of transmembrane segments V and VI, respectively, Zn^{2+} inhibits binding of radiolabelled agonist peptide and efficiently blocks phosphoinositol turnover induced by substance P. We propose that Zn^{2+} and CP96,345 act as 'allosteric competitive' antagonists by stabilizing inactive conformations of the mutant and the wild-type receptor respectively. Introduction of metal-ion-binding sites could be used as a general tool in the structural and functional characterization of helix–helix interactions in G-protein-coupled receptors, as well as in other membrane proteins.

On the basis of the apparent spatial proximity of the putative contact points for CP96,345 in the molecular model of the human NK-1 receptor (Fig. 1), we attempted to exchange the binding site for the non-peptide antagonist with a metal-ion-binding site in order to test this model and the mechanism of action of the non-peptide antagonist[11,14] by using a considerably smaller and structurally unrelated metal-ion. The structures of several naturally occurring metal ion sites are known[15–17] and similar sites have been built into other proteins and into model proteins[18–20]. Histidine residues were incorporated at selected positions in and around the putative binding site for CP96,345 and the ability of the non-peptide antagonist and Zn^{2+} to inhibit the binding of radiolabelled substance P (the natural peptide agonist) was monitored. One of the suggested interaction points in transmembrane segment V (TM-V) is already a histidine, namely His 197 (HisV:05)[2]. Substitution of Glu 193 (GluV:01), one helical turn above this point, with a histidine increased the

TABLE 1 Binding of peptide agonist, non-peptide antagonist and metal ions to wild-type and histidine-substituted NK-1 receptor mutants

		Substance P				CP96,345				$ZnCl_2$				$CuCl_2$			
	Helical segment	K_d (nM)	±s.e.m.	(*n*)	F_{mut}	K_i (nM)	±s.e.m.	(*n*)	Fold decrease	K_i (μM)	±s.e.m.	(*n*)	Fold increase	K_i (μM)	±s.e.m.	(*n*)	Fold increase
hNK-1		0.21	±0.02	(13)	1.0	0.25	±0.02	(10)	1	492	±42	(7)	1	346	±49	(6)	1
[E193H]	TM-V	0.12	±0.01	(8)	0.6	1.54	±0.09	(5)	6	11	±2	(5)	44	116	±24	(4)	3
[T201H]	TM-V	0.23	±0.05	(4)	1.1	14.2	±3.2	(3)	57	50	±0	(3)	10	49	±23	(2)	7
[F268H]	TM-VI	0.52	±0.08	(6)	2.5	1.17	±0.19	(3)	5	38	±2	(5)	13	42	±20	(2)	8
[L269H]	TM-VI	0.11	±0.01	(7)	0.5	0.41	±0.03	(5)	2	73	±3	(5)	7	167	±18	(4)	2
[Y272H]	TM-VI	0.05	±0.01	(9)	0.2	0.50	±0.05	(5)	2	5	±1	(5)	94	393	±49	(5)	1
[F268H;Y272H]	TM-VI	0.74	±0.31	(3)	3.5	4.00	±0.97	(4)	16	4	±1	(4)	123	313	±32	(2)	1
[L269H;Y272H]	TM-VI	0.05	±0.01	(5)	0.2	6.12	±1.23	(3)	24	17	±0	(3)	29	329	±60	(2)	1
[E193H;F268H]	TM-V and -VI	1.41	±0.46	(5)	6.7	6.00	±1.45	(3)	24	19	±1	(5)	26	133	±79	(2)	3
[E193H;L269H]	TM-V and -VI	0.15	±0.02	(7)	0.7	5.63	±0.65	(4)	23	12	±2	(5)	40	63	±15	(4)	5
[E193H;Y272H]	TM-V and -VI	0.34	±0.04	(14)	1.6	34.3	±5.8	(8)	137	0.62	±0.10	(7)	794	37	±10	(6)	9
[H197A]	TM-V	0.12	±0.02	(6)	0.6	33.2	±2.7	(4)	133	1,517	±268	(5)	0.3	399	±55	(6)	1
[H265A]	TM-VI	0.10	±0.02	(6)	0.5	0.29	±0.04	(4)	1	112	±7	(6)	4	185	±40	(6)	2

Gradual conversion of the putative binding site for the non-peptide antagonist CP96,345 to a Zn^{2+}-binding site by substitution with His residues. Construction of receptor mutants: residues in the human (h) NK-1 receptor were selected for His substitution on the basis of previous mutational analysis of the CP96,345-binding site[1–5] plus neighbouring residues Thr 201 and Leu 269, and on the structure of natural and artificial metal-ion sites[16,18]. Mutants were constructed using oligonucleotide-directed mutagenesis and recombinant polymerase chain reaction (PCR)[28]. cDNAs encoding wild-type and mutant receptors were cloned into a pTEJ-8 expression vector[29]; all mutations were verified by restriction endonuclease mapping and DNA sequence analysis. Cloned receptors were transiently expressed in COS-7 cells transfected by calcium phosphate precipitation 2 days before the binding assay[30]. Binding was assayed using whole cells at 4 °C and 40 pM mono-iodinated ^{125}I-Bolton Hunter substance P (^{125}I-BH-SP) as described[30]. Determinations were made in triplicate (SP, CP96,345) or duplicate ($ZnCl_2$, $CuCl_2$). Binding data were analysed and IC_{50} values determined by nonlinear regression analysis using the Inplot 4.0 software (GraphPad Software, San Diego). Values of the dissociation and inhibition constants (K_d and K_i) were estimated from competition binding using the equations $K_d = IC_{50} - L$ and $K_i = IC_{50}/(1 + L/K_d)$, where L is the concentration of radioligand.